Cytotherapy 25 (2023) 210–219

Contents lists available at ScienceDirect

CYTOTHERAPY

journal homepage: www.isct-cytotherapy.org

FULL-LENGTH ARTICLE
Manufacturing

# Development of a personalized dendritic cell vaccine and single-cell RNA sequencing–guided assessment of its cell type composition

Qingli Li[1,#], Chao Yang[1,#], Huan Tian[2], Jinfeng Jiang[3], Ping Li[1], Xiaofeng Zhu[1], Tingjun Lei[4], Rutie Yin[1], Ping Ding[3], Peng Bai[2,*], Qintong Li[1,**]

[1] *Departments of Obstetrics & Gynecology and Pediatrics, West China Second University Hospital, Key Laboratory of Birth Defects and Related Diseases of Women and Children, Ministry of Education, Development and Related Diseases of Women and Children Key Laboratory of Sichuan Province, Center of Growth, Metabolism and Aging, College of Life Sciences, State Key Laboratory of Biotherapy and Collaborative Innovation Center of Biotherapy, Sichuan University, Chengdu 610041, Sichuan, China*
[2] *Department of Forensic Genetics, West China School of Basic Medical Sciences & Forensic Medicine, Sichuan University, Chengdu 610041, Sichuan, China*
[3] *Non-coding RNA and Drug Discovery Key Laboratory of Sichuan Province, Chengdu Medical College, Chengdu 610500, Sichuan, China*
[4] *Division of Immunology, Sichuan Cunde Therapeutics, Chengdu 610093, Sichuan, China*

ARTICLE INFO

*Article History:*
Received 14 June 2022
Accepted 28 October 2022

*Key words:*
CUD-002
Dendritic cell
Manufacturing
Neoantigen
Ovarian cancer
Single-cell analysis

ABSTRACT

*Background aims:* Dendritic cell (DC)-based immunotherapy is a promising approach to treat cancer; however, there is no consensus on the manufacturing processes. Cell type heterogeneity in products manufactured by various methods is understudied and may elicit safety concerns from the regulatory perspective.
*Methods:* We characterized the cell type composition of a recently developed DC vaccine, CUD-002, consisting of DCs loaded with mRNA encoding personalized tumor neoantigens (NCT05270720).
*Results:* Using single-cell transcriptomic analysis as an unbiased approach, we found that >80% cells in the final product were DCs and the rest primarily comprised myelocytes and lymphocytes. Subsequent fluorescence-activated cell sorting analyses confirmed these cellular identities. These results indicate that unintended cells originate from leukapheresis, the first step of the manufacturing process, and thus likely safe. Consistently, no overt toxicity or tumorigenicity was observed in mice inoculated with CUD-002.
*Conclusions:* Considering that leukapheresis is a widely used procedure for collecting diverse peripheral blood cell types to manufacture various cytotherapies, this study establishes a workflow to analyze and address regulatory considerations on cell type heterogeneity.


## Introduction

Dendritic cell-based immunotherapy is an approved treatment for prostate cancer and is under clinical evaluation for a variety of human cancers [1]. Endogenous dendritic cells are the most proficient antigen-presenting cells to display tumor antigens and play an essential role in anti-tumor immunity [2]. However, it is impractical to isolate a sufficient amount of endogenous dendritic cells for autologous cell therapies [3]. To manufacture dendritic cells on an industrial scale, the most popular approach is to collect peripheral blood monocytes via leukapheresis. Enriched monocytes can be further purified by elutriation based on the physical properties of monocytes or by the affinity to lineage-specific antibodies. Purified monocytes are then cultured by various methods to generate dendritic cells [4]. At the final step of the manufacturing process, different methods are used to load dendritic cells, such as mRNA electroporation and incubation with peptide, recombinant protein or tumor cell lysate [5]. A prominent example is Sipuleucel-T, also known as PROVENGE or Dendreon, the first therapeutic dendritic cell vaccine approved by the US Food and Drug Administration to treat metastatic castration-resistant prostate cancer with no or minimal symptoms [6].

* Correspondence: Peng Bai, Department of Forensic Genetics, West China School of Basic Medical Sciences & Forensic Medicine, Sichuan University, Chengdu 610041, Sichuan, China.
** Correspondence: Qintong Li, Departments of Obstetrics & Gynecology and Pediatrics, West China Second University Hospital, Key Laboratory of Birth Defects and Related Diseases of Women and Children, Ministry of Education, Development and Related Diseases of Women and Children Key Laboratory of Sichuan Province, Center of Growth, Metabolism and Aging, College of Life Sciences, State Key Laboratory of Biotherapy and Collaborative Innovation Center of Biotherapy, Sichuan University, Chengdu 610041, Sichuan, China.
*E-mail addresses:* baipeng@scu.edu.cn (P. Bai), liqintong@scu.edu.cn (Q. Li).
# These authors contributed equally to this work.

https://doi.org/10.1016/j.jcyt.2022.10.013

Notably, there is still no consensus on the optimal way to manufacture dendritic cells for cancer therapy [7]. Variations on donor materials and manufacturing methods inevitably result in heterogeneity in cell-type compositions in the final products. For regulatory considerations, it is important to define the cell-type composition to address safety concerns but also to ensure reproducible, high-quality manufacturing of intended cell type. Fluorescence-activated cell sorting (FACS) analysis frequently is used to immunophenotype cell types. However, it requires previous knowledge of the cell types in the products and offers limited information on functional cellular states. Thus, other methodologies are needed to characterize the heterogenous cell types in an unbiased manner.

Ovarian cancer has been the most lethal gynecologic cancer during the past decade and remains a high unmet medical need worldwide. High mortality is partly the result of a long-standing paucity of effective therapies other than platinum-based chemotherapy [8]. Interestingly, two decades ago, tumor-infiltrating T cells were demonstrated in many patients with ovarian cancer [9]. However, recent large-scale phase 2 and 3 clinical trials with immune checkpoint inhibitors including anti-programmed cell death protein 1 (anti-PD-1, pembrolizumab) and anti-programmed death-ligand 1 monoclonal antibodies (anti-PD-L1, atezolizumab and avelumab) failed to achieve meaningful efficacy in patients with ovarian cancer, either as standalone or combined with stand-of-care therapeutic agents [10–12]. These observations indicate that the priming phase of anti-tumor immunity by dendritic cells may be deficient in ovarian cancer [13,14].

We recently developed a versatile dendritic cell-based platform, CUD-002, consisting of Good Manufacturing Practice (GMP)-grade dendritic cells loaded with *in vitro*–transcribed mRNA encoding personalized neoantigens. CUD-002 exhibits favorable efficacy in preclinical cellular and animal models to treat ovarian cancer and is currently under evaluation in phase I clinical trial (NCT05270720). Here, we demonstrate a reproducible production of high-quality CUD-002 product and use single-cell transcriptomic sequencing as an unbiased approach to characterize cell type compositions in CUD-002 and to guide the development of FACS-based method as quality assurance and control steps in the manufacturing process.

## Methods

### *Leukapheresis*

To develop a GMP manufacturing process, peripheral blood mononuclear cells were collected by leukapheresis at West China Second University Hospital of Sichuan University. Informed consent was obtained from all volunteers for apheresis donation, and this study was approved by the Ethical Committees of West China Second University Hospital at Sichuan University. A single collection from health donors (median age: 33 years; range: 19–56 years; 66 male and 19 female donors) using Spectra Optia system (Terumo BCT, Lakewood, CO, USA) with the mononuclear cell collection procedure was made.

### *Enrichment of monocytes by elutriation*

Continuous-counterflow elutriation was performed with the Elutra system (Terumo BCT) in Hanks' buffered salt solution (Lonza, Basel, Switzerland) supplemented with 1% human albumin. After priming with Hanks' buffered salt solution, the leukapheresis product was loaded via the inlet pump into the constantly rotating elutriation chamber, using a constant centrifugation speed of 2400 rpm and increasing the cell medium flow rate step-by-step (37 mL/min, 97.5 mL/min, 97.5 mL/min, 97.5 mL/min, 103.4 mL/min and 100 mL/min). The total elutriation time was 1 h. Six fractions were collected, and the percentage of various immune cells was analyzed by ABX Pentra 60 hematology analyzer (HORIBA, Irvine, CA, USA). The cellular viability was measured using flow cytometry (Accuri C6 Plus; Beckman Coulter Life Sciences, Indianapolis, IN, USA) by staining with propidium iodide and anti-CD45 antibody (BD Biosciences, San Diego). The percentage of monocytes was determined using flow cytometry (Accuri C6 Plus; Beckman Coulter Life Sciences) by labeling with propidium iodide and anti-CD14 antibody (BD Biosciences). In most circumstances, monocytes were enriched in fractions 4, 5 or 6. At least $10^9$ monocytes were cultured to generate dendritic cells. Due to variations on donor materials, monocytes from single-fraction or combined fractions were used. Of 85 batches produced, 42 were manufactured using faction 6 alone, 35 from combined fractions 5 and 6, 4 from combined fractions 4, 5 and 6, 3 from fraction 5 alone and 1 from combined fractions 4 and 5.

### *Generation of dendritic cells*

Monocytes were cultured in gas-permeable plastic bags (Corning, Corning, NY, USA) at a density of 5 × 105 cells/mL in AIM-V (Gibco/Thermo Fisher Scientific, Waltham, MA, USA) supplemented with 800 U/mL granulocyte-macrophage colony-stimulating factor (R&D Systems, Minneapolis, MN, USA) and 500 U/mL interleukin-4 (R&D Systems) for 5 days, followed by the addition of 10 ng/mL recombinant human tumor necrosis factor-$\alpha$ (R&D Systems), 5 ng/mL recombinant human interferon (IFN)-$\gamma$ (R&D Systems) and 2.5 $\mu$g/mL PGE2 (Cayman Chemical Company, Ann Arbor, MI, USA) into the culture bag. Mature dendritic cells were collected by centrifugation (300 x g) at day 7. For electroporation with in vitro transcribed mRNA, dendritic cells were resuspended in 4-mm gap cuvettes using the Gene Pulser X cell Electroporation System (Bio-Rad, Hercules, CA, USA) with proprietary parameters. After electroporation, cells were cultured for 4 h, collected by centrifugation, resuspended in CS10 (STEMCELL Technologies) and aliquoted in Daikyo Crystal Zenith Vials (West, Exton, PA, USA; $10^7$ cells/vial). Each vial was placed in a CryoMed controlled-rate freezer (Thermo Fisher Scientific) until temperature reached to −130°C, then transferred to the liquid phase of liquid nitrogen for long-term storage until the day of distribution.

### *Cell counting and immunophenotyping analyses*

The quantity and percentage of various immune cell types in leukapheresis product and elutriation fractions were analyzed by an ABX Pentra 60 hematology analyzer (HORIBA). For other experiments, FACS analysis (Accuri C6 Plus; Beckman Coulter Life Sciences) was used. Monocytes were enumerated by $CD45^+/CD14^+$ and propidium iodide–negative population (Beckman Coulter Life Sciences). Dendritic cells were gated by forward scatter and side scatter on the basis of cell size and cellular complexity, and further gated by anti-CD45 and propidium iodide. Phenotypic analyses of dendritic cells were performed using anti-CD209-APC, CD80-PE, CD83-PE, CD86-PE, CD11c-PE, HLA-DR-APC, HLA-ABC-APC and CCR7-APC (Beckman Coulter Life Sciences). To analyze cell type compositions in CUD-002 product, anti-CD45-APC, CD19-PE, CD20-PE, CD3-Percp-Cy5.5, CD56-PE, CD34-PE, lineage cocktail (CD3/CD14/CD16/CD19/CD20/CD56)-FITC, CD13-PE, CD33-PE and S100A9-PE (Beckman Coulter Life Sciences) were used.

### *Single-cell transcriptomic analysis*

Cell suspension (20 $\mu$L, 106/mL, viability >95%) was loaded into Chromium microfluidic chips with 3′ reagent kit (v3.1 chemistry), and barcoded with a 10x Chromium Controller (10X Genomics, Pleasanton, CA, USA). RNA from the barcoded cells was subsequently reverse-transcribed and sequencing libraries constructed with reagents from a Chromium Single Cell 3′ v3.1 reagent kit (10X Genomics) following manufacturer's instructions. Sequencing was performed using Illumina NovaSeq platform following manufacturer's

instructions. In total, 25,718 single cells from two healthy donors were analyzed. On average, approximately 45,000 reads were generated per cell by Illumina NovaSeq PE150. Raw binary base call files were converted to FASTQ files, aligned to human GRCh38 reference genome to produce sparse gene expression matrix by CellRanger v3.0 pipeline [15]. To filter out low-quality data, cells with percentage of counts in mitochondrial genes over 30% and with less than 100 genes or 200 UMI were removed from downstream analyses [16]. Potential cell doublets were identified by DoubletFinder and removed downstream analyses [17]. The expression matrix generated by CellRanger v3.0 was further processed and analyzed by Seurat v4.0. SCTransform to normalize UMI counts in each cell [18]. Percentage of counts in mitochondrial genes and cell cycle scores were regressed out using vars.to.regress. variable.features.n was set to 5000 for the following analysis. Fifty principal components were calculated and their significances were tested using ElbowPlot [18]. The top 30 principal components were analyzed by Seurat v4.0. FindNeighbors and uniform manifold approximation and projection (UMAP) visualization [19]. Batch effects were corrected using the Harmony package in UMAP visualization. Differentially expressed genes in each cell cluster were identified by Seurat v4.0 FindAllMarkers ($\log_2$(fold change) > 0.5, min.pct = 0.5), and visualized using Seurat v4.0 DoHeatmap. Wilcoxon rank-sum test was used to compute *P*-values adjusted for multiple testing using the Benjamini–Hochberg correction. To assign cell identity for each cluster, SingleR package was used to annotate the most plausible cell types, and marker genes were used to confirm their identities manually.

*Functional analyses of the efficacy of CUD-002*

CUD-002 products were co-cultured with autologous $CD8^+$ T cells in AIM-V (Gibco/Thermo Fisher Scientific) supplemented with interleukin-2 (20 U/mL) for 14 days. The functionality of CUD-002-stimulated T cells was analyzed by three assays. First, the percentage of neoantigen-specific $CD8^+$ T cells was determined by the major histocompatibility complex tetramer staining assay following manufacturer's instruction (MBL, Tokyo, Japan). To summarize, the stimulated $CD8^+$ T cells were harvested and stained with PE-conjugated MART-1 peptide/HLA-A0201 tetramer (MBL) as well as fluorescein isothiocyanate–conjugated anti-human CD8 (BD Biosciences), and then were analyzed by flow cytometry (BD Biosciences). Second, the ability of neoantigen-specific $CD8^+$ T cells to secret IFN-$\gamma$ was measured by an automated ELISPOT reader (Cellular Technology Ltd., Shaker Heights, OH, USA). Third, neoantigen-specific CD8+ T cells were examined for their abilities to kill OVCAR-8 ovarian cancer cells in a cytotoxicity assay. To summarize, $CD8^+$ T cells were incubated with OVCAR-8 ovarian cancer cells loaded with MART-1 peptide for 24 h. OVCAR-8 were also stably transfected with red fluorescent protein (mCherry) to facilitate its detection by FACS analysis.

*Tumorigenicity assessment*

To examine the tumorigenic potential of CUD-002 products, NOD/SCID mice (Beijing Vitalstar Biotechnology Co., Ltd., Beijing, China) were used with equal number of 7- to 8-week-old male and female mice. In accordance with the China National Medical Products Administration (NMPA) guidelines, this experiment was carried out by an independent contractor, JOINN Laboratories, Suzhou, China, under the Organisation for Economic Co-operation and Development (OECD) principles of Good Laboratory Practice in an Association for Assessment and Accreditation of Laboratory Animal Care (AAALAC)–accredited animal research facility. Each mouse was subcutaneously injected with a single dose of CUD-002 product containing $1 \times 10^7$ dendritic cells ($4 \times 10^8$ cells/kg for a 25 g mouse) (n = 24). This quantity of dendritic cells will be used in human patients in the clinical trial (NCT05270720). As a positive control, six male and six female mice were subcutaneously injected with Hela cells (single dose of $1 \times 10^6$ Hela cells per mouse). Subsequently, all animals were assessed for body weight, macroscopic and microscopic changes, and tumor masses. Animals injected with HeLa cells were sacrificed after 56 days, due to tumor volume approaching 1 $cm^3$. Animals injected with CUD-002 products were observed till 112 days. All masses formed at the site of injection were isolated and assessed by histopathology. None of mice injected with CUD-002 product formed any detectable tumor.

*Toxicity assessment*

NOG-dKO mice (Charles River Laboratories, Beijing, China) were used with an equal number of 9-week-old male and female mice. The experiment was carried out by an independent contractor, JOINN Laboratories, Suzhou, China, under the OECD principles of Good Laboratory Practice in an AAALAC-accredited animal research facility. The potential toxicity profiles of CUD-002 product were assessed after repeated intravenous slow bolus injections in NOG-dKO mice (n = 60). Two doses were examined, containing $3 \times 10^5$ or $3 \times 10^6$ dendritic cells, respectively ($1.2 \times 10^7$ or $1.2 \times 10^8$ cells/kg for a 25-g mouse, respectively). Dendritic cells were injected weekly for eight consecutive weeks. Eight doses were chosen because human patient will receive eight doses of CUD-002 (NCT05270720). During a period of 64 days, animals were constantly monitored and assessed for clinical signs, body weight, food consumption, functional and behavioral changes, clinical pathology such as clinical chemistry parameters (A/G ratio (calculated), alanine aminotransferase, albumin, alkaline phosphatase, aspartate aminotransferase, bilirubin (total), calcium, chloride, cholesterol (total), creatinine, globulin (calculated), glucose, phosphorus (inorganic), potassium, protein (total), sodium, triglycerides, urea; urinalysis: blood, pH, glucose, protein, urobilinogen, ketones, bilirubin, color and appearance, specific gravity, volume). At the end of the observation time, macroscopic changes and organ weights were recorded, and organs were subjected to histopathology examination.

## Results

*An overview of the CUD-002 manufacturing process*

An overview of the CUD-002 manufacturing process is shown in Figure 1A. To develop a personalized dendritic cell–based therapy, the manufacturing process was developed and optimized using peripheral blood monocytes collected by leukapheresis and enriched by subsequent elutriation (day 1). Enriched monocytes were differentiated in culture bags to generate dendritic cells, followed by electroporation of *in vitro*–transcribed mRNA encoding personalized neoantigens and an ovarian cancer–associated antigen (days 2-7). Various quality assurance and control analyses as well as microbiological examinations (days 7-28) were carried out in accordance with GMP guidelines from the China National Medical Products Administration (NMPA, formerly known as the China Food and Drug Administration) (Figure 1A).

To develop a robust manufacturing process to enrich monocytes, we carried out 85 test runs. Monocytes in peripheral blood from 85 healthy volunteers were collected by leukapheresis using the Spectra Optia apheresis system. The percentage of monocytes ranged from 8.8% to 41.9% (median: 21.1%; mean: 21.8 ± 0.1%), quantified by an ABX Pentra 60 hematology analyzer (Figure 1B). Monocytes collected by leukapheresis were further purified using the Elutra system, resulting in a median of 74.3% monocytes (range: 60.3–89.3%; mean: 74.1±0.1%) (Figure 1C). The identity of purified monocytes was verified by FACS analysis ($CD14^+$) (Figure 1D). These monocytes were then differentiated into dendritic cells in culture bags. In most circumstances, monocytes were enriched in fractions 4, 5 or 6 (Figure 1E). At least $10^9$ monocytes were cultured to generate dendritic cells. Due to variations on donor materials, monocytes from single-fraction or

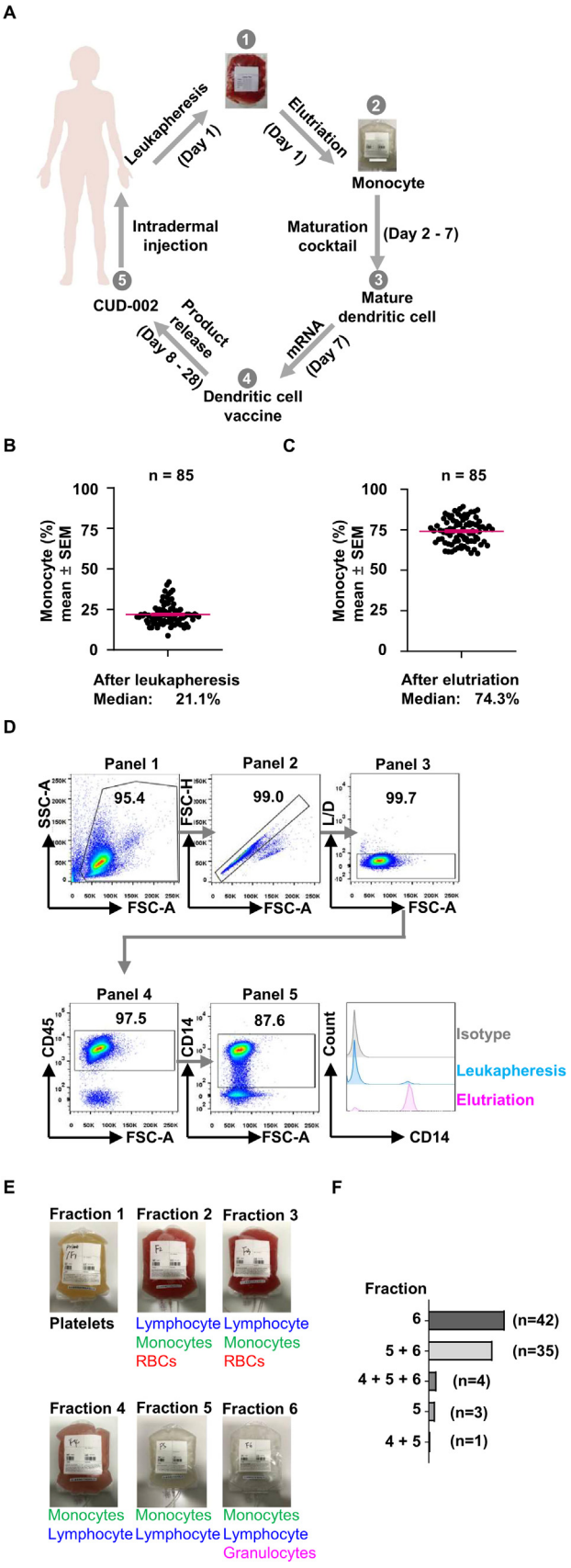


**Figure 1.** Analysis of monocytes purified by leukapheresis and elutriation. (A) An overview of the manufacturing process of newly developed dendritic vaccine, CUD-002. In summary, periphery blood monocytes are collected by leukapheresis and elutriation (day 1) and used to generate dendritic cells followed by electroporation with mRNA encoding personalized neoantigen (day 7). The CUD-002 product is subjected to various quality control steps (day 7-28) before intradermal injection into patients. (B) The percentage of monocytes in leukapheresis product determined by ABX Pentra 60 hematology analyzer from 85 test runs. (C) The percentage of monocytes in elutriation product determined by ABX Pentra 60 hematology analyzer from 85 test runs. (D) Analysis of the percentage of monocytes after leukapheresis and elutriation. Gating strategy of FACS using anti-CD14 antibody for elutriation product was shown. Cells were gated based on side scatter area (SSC-A) and forward scatter area (FSC-A) (panel 1), then gated to include singlet (panel 2) and live cells (panel 3). CD45+ cells (panel 4) were further gated to identify CD14+ monocytes (panel 5). An example of the comparison of monocyte purity after leukapheresis and elutriation was shown (panel 6). (E) Example of fractions separated by elutriation. Cellular components determined by ABX Pentra 60 hematology analyzer were shown for each fraction. (F) Statistics of elutriation fractions used to generate dendritic cells. 85 donor materials were used. Due to donor variations, monocytes from single or combined fractions were used. (Color version of figure is available online.)

combined fractions were used. Of 85 batches produced, 42 were manufactured using faction 6 alone, 35 from combined fractions 5 and 6, 4 from combined fractions 4, 5 and 6, 3 from fraction 5 alone, and 1 from combined fractions 4 and 5 (Figure 1F).

Several quality-control steps were carried out to ensure the quality of manufactured dendritic cells. Microscopic inspection revealed that most cells had a high surface-to-volume ratio and contained multiple cytoplasmic projections characteristic of dendritic cell morphology (Figure 2A). Immunophenotyping by FACS analysis was carried out to verify the identity ($CD11c^+$, $HLA\text{-}DR^+$ and $CD209^+$), the maturation state ($CD80^+$, $CD83^+$, $CD86^+$ and $HLA\text{-}ABC^+$) and the migratory ability ($CCR7^+$) of dendritic cells (Figure 2B). No residue monocytes were detected (lack of $CD14^+$ cells) (Figure 2B). In 72 manufactured batches, the median percentage was 91.0% for $CD209^+$ (range: 63.0–100%; mean: 88.7 ± 0.13%), 99.0% for $CD80^+$ (range: 83.0–100%; mean: 91.0 ± 0.05%), 93.0% for $CD83^+$ (range: 75.0–100%; mean: 74.1 ± 0.1%), 100% for $CD86^+$ (range: 95.3–100%; mean: 99.6 ± 0.01%), 80.0% for $CCR7^+$ (range: 60.0–97.0%; mean: 78.9 ± 0.12%) and 100% for $HLA\text{-}ABC^+$ (range: 96.0–100%; mean: 99.9 ± 0.01%) in the dendritic cell population by FACS analysis (Figure 2C). The median cellular viability was 91.0% (range: 79.0–99.2%; mean: 90.0 ± 0.1%) (Figure 2D). The median yield of dendritic cell per monocyte was 35.4% (range: 12.6–71.4%; mean: 36.3 ± 0.2%) (Figure 2E). Among donors, the yield was positively proportional to the quantity of monocytes at the beginning of culturing process (Figure 2F).

### *Single-cell transcriptomic analysis of CUD-002 cell type compositions*

To dissect cell type compositions in an unbiased manner, we carried single-cell transcriptomic analysis of CUD-002 products from two donors. In total, 13,790 and 11,928 cells were profiled using droplet-based single-cell RNA sequencing (Chromium; 10x Genomics) for donor 1 and donor 2, respectively. After quality control, high-quality sequencing data were obtained containing 11,887 and 10,025 cells for donor 1 and donor 2, respectively. All cells were integrated and subjected to donor correction by Harmony [20]. Twenty distinct clusters were identified by unsupervised clustering using the Louvain method [21]. Cell types were first calculated using the SingleR package [22], assigned with the most differentially expressed marker genes using Seurat [18], and then annotated by highly lineage-specific canonical markers. These analyses generated six distinct cell groups. Top 20 representative marker genes using z-score calculation were illustrated in a heatmap for non-dendritic cell types (Figure 3A). In total of 5751 bystander cells, the expression levels of top five marker genes per bystander cell type were illustrated (Figure 3B). Uniform manifold approximation and projection visualization of these cells revealed that the majority of cells were identified as dendritic cell (91.61% and 90.54% for donor 1 and 2, respectively) (Figure 3C). The percentage of remaining immune cell types included 3.63% and 4.12% T cells, 2.73% and 3.74% myelocytes, 1.46% and 0.82% B cells, 0.56% and 0.71% natural killer cells (NK), 0.32% and 0.33% hematopoietic stem cells (HSC) for donor 1 and 2, respectively (Figure 3C). Harmony integration demonstrated that samples from different donors were well mixed and grouped by defined cell types (Figure 3D). We

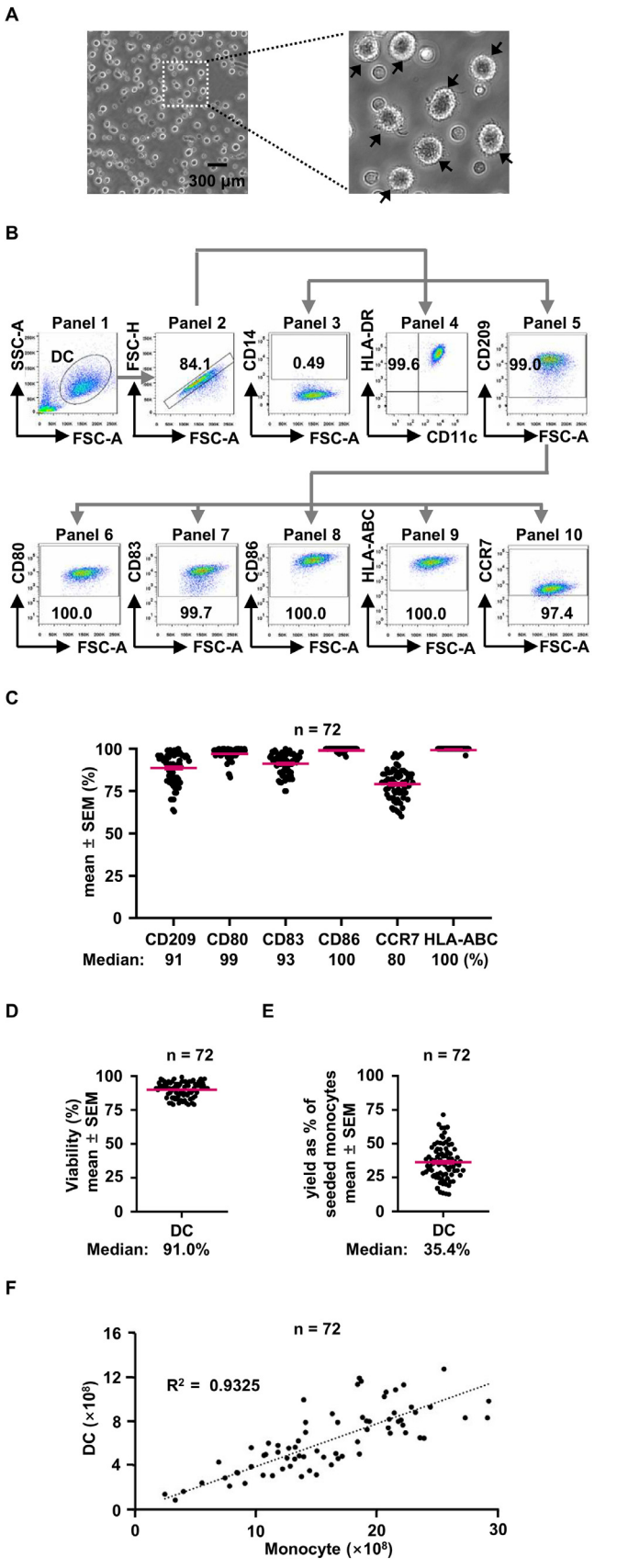


**Figure 2.** A reproducible production of GMP-grade CUD-002. (A) Microscopic examination of CUD-002 product. Dendritic cells are denoted with an arrow. (B) Phenotyping of CUD-002 by FACS analysis. FACS analysis was carried out to verify the identity (CD11c$^+$, HLA-DR$^+$ and CD209$^+$), the maturation state (CD80$^+$, CD83$^+$, CD86$^+$ and HLA-ABC$^+$) and the migratory ability (CCR7$^+$) of dendritic cells. Dendritic cells (DC) were gated based on side scatter area (SSC-A) and forward scatter area (FSC-A) (panel 1), then gated to include singlet cells (panel 2). Cells from panel 2 were further gated to identify CD14$^+$ monocytes (panel 3), HLA-DR$^+$/CD11c$^+$ dendritic cells (panel 4) and CD209$^+$ dendritic cells (panel 5). Because HLA-DR$^+$/CD11c$^+$ and CD209$^+$ identified virtually the same population, CD209$^+$ was used as a phenotypic marker for dendritic cells in manufacturing process. CD209$^+$ dendritic cells (panel 5) were further gated to identify the percentage of CD80$^+$ (panel 6), CD83$^+$ (panel 7), CD86$^+$ (panel 8), HLA-ABC$^+$ (panel 9), and CCR7$^+$ (panel 10) cells. (C) Phenotyping of 72 batches of CUD-002 product using FACS analysis as in (B). (D) Viability of 72 batches of CUD-002 product determined FACS analysis. (E) The yield of dendritic cells from 72 batches of CUD-002 product. (F) Correlation analysis between the quantity of monocytes and generated dendritic cells from 72 batches of CUD-002 product. (Color version of figure is available online.)

analyzed dendritic cell markers for maturation (CD80, CD83 and CD86) and the migratory abilities (CCR7). These markers were highly expressed in DC population by single-cell analysis (Figure 3E).

### *Verification of CUD-002 cell type composition by FACS analysis*

To verify cell types identified by single-cell transcriptomic analysis (Figure 3), we carried out direct comparison of each cell type between starting material and product from these two donors using FACS analysis. Gating strategies for dendritic cell (Figure 4A), T (Figure 4B), NK, B, HSC and myelocyte (Figure 4C) in CUD-002 were shown. In CUD-002 product manufactured from donor 1 material, the frequencies of immune cells were 92.5% dendritic cells, 5.2% myelocytes, 0.6% T cells, 1.6% B cells, 0.10% NK cells and 0.044% HSCs. For donor 2, the frequencies of immune cells were 88.2% dendritic cells, 9.0% myelocytes, 1.0% T cells, 1.6% B cells, 0.175% NK cells and 0.012% HSCs (Figure 4D). These results also demonstrate a high concordance in cell type composition and frequency between single-cell sequencing and FACS analysis. Thus, we integrated FACS analysis of these cell types into quality-control procedures. As an example, analyses of CUD-002 product manufactured from additional 10 donor materials were shown. The median frequencies of immune cells were 85.3% dendritic cells (range: 80.7–93.2%; mean: 86.9 ± 0.4%), 9.2% myelocytes (range: 3.9–16.2%; mean: 8.6 ± 0.4%), 3.1% T cells (range: 0.6–6.5%; mean: 2.5 ± 0.2%), 1.1% B cells (range: 0.3–5.0%; mean: 1.8 ± 0.2%), 0.10% NK cells (range: 0–0.1%; mean: 0.1 ± 0.005%) and 0.10% HSCs (range: 0–0.4%; mean: 0.1 ± 0.007%) (Figure 4E).

To trace the origin of theses bystander cell types, we analyzed their percentages in leukapheresis and elutriation products. Gating strategies for T (Figure 4F), NK, B, HSC and myelocyte (Figure 4G) in elutriation product are shown. The frequencies of immune cells for donor 1 were 59.5% monocytes (CD14$^+$), 27.9% granulocytes (CD16$^+$), 7.7% myelocytes (negative for lineage cocktail containing CD3/CD14/CD16/CD19/CD20/CD56, and positive for CD13/CD33/S100A9), 2.4% T cells (CD3$^+$), 2.3% B cells (CD19/CD20$^+$), 0.015% NK cells (CD56$^+$) and 0.197% HSCs (negative for lineage cocktail containing CD3/CD14/CD16/CD19/CD20/CD56, and positive for CD34). For donor 2, the frequencies were 67.6% monocytes, 14.8% granulocytes, 13.5% myelocytes, 1.8% T cells, 2.0% B cells, 0.004% NK cells and 0.237% HSCs (Figure 4H). Interestingly, the percentage of myelocyte was similar in elutriation product and CUD-002 derived from donor 1 and 2 (Figure 4D and 4H), indicating that myelocyte might not arise from the culturing process. We further analyzed the percentage of myelocyte in leukapheresis product (Figure 4I). The frequency of myelocyte was 0.01% and 0.02% for donor 1 and 2, respectively (Figure 4J). Because elutriation is a separation method by physical force, these results indicate that myelocyte is originated from leukapheresis and further enriched by elutriation.

### *Non-dendritic cell types in CUD-002 do not impair the efficacy of dendritic cells*

To address whether bystander cells in CUD-002 might interfere with dendritic cell function, we chose two CUD-002 products

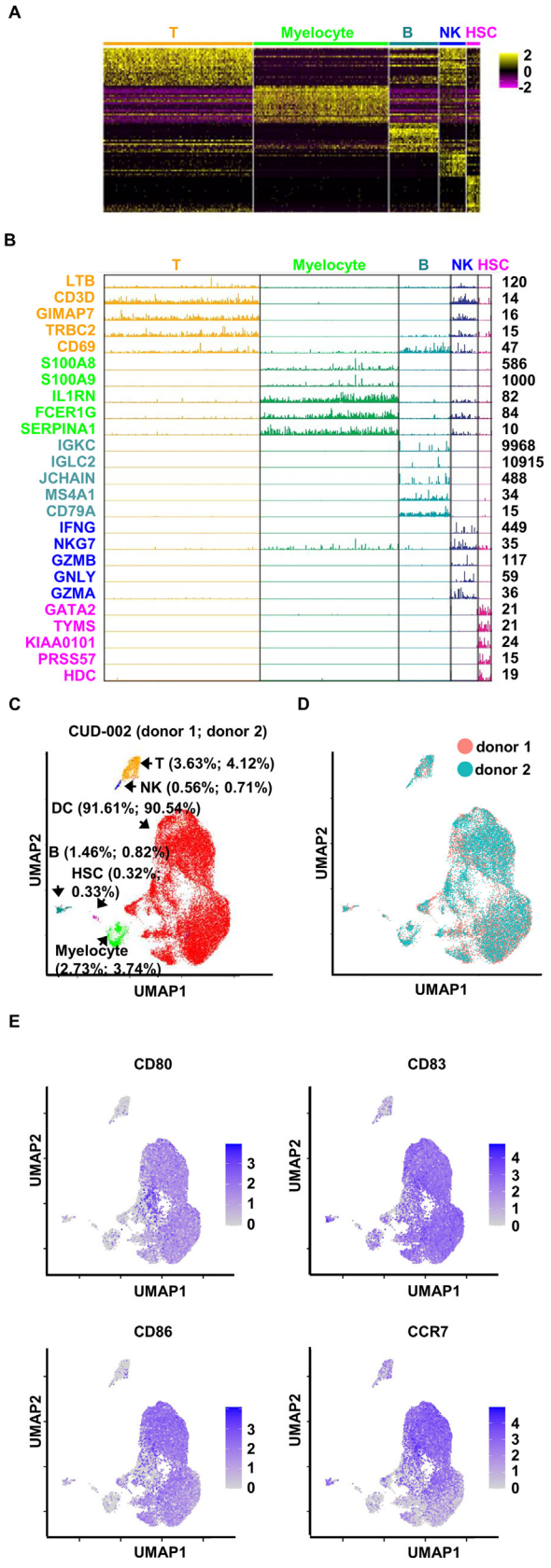


**Figure 3.** Single-cell transcriptomic analysis of the cell type composition in CUD-002. (A) Heatmap presentation of five non-dendritic cell (DC) types in CUD-002, classified by top 20 differentially expressed genes using z-score calculation. (B) Expression levels of marker genes in 5,751 bystander cells. Top 5 marker genes for each cell type were presented. Numbers on the right denote maximum detected expression by single-cell analysis. (C) UMAP visualization of six cell types in CUD-002 manufactured from two donors (21,912 cells). Numbers in parenthesis denote the frequency of indicated cell types from donor 1 and donor 2, respectively. (D) UMAP visualization of 21,912 cells from two donors after Harmony integration. (E) Expression levels of markers for DC maturation (CD80, CD83 and CD86) and the migratory abilities (CCR7). Side bar denotes relative expression level. (Color version of figure is available online.)

containing relatively high myelocyte content (8.7% and 13.9% for donor 3 and 4, respectively) (Figure 5A). We used anti-CD209 to affinity purify dendritic cells from CUD-002 product (purity >99% by FACS analysis). We compared unpurified cells (CUD-002) and purified cells (purified DC) in their abilities to stimulate antigen-specific T-cell response using MART-1 as a model antigen (Figure 5B). For donor 3, CUD-002 stimulated slightly more MART-1–specific T cells than purified DC. For donor 4, CUD-002 and purified cells had similar efficiency. Consistently, in the enzyme-linked immunospot (ELISPOT) assay, MART-1–specific T cells secreted similar amounts of IFN-$\gamma$ (Figure 5C). In addition, we retrospectively analyzed our pre-clinical data that have pairwise information on the percentage of non- dendritic cells (FACS analysis), percentage of neoantigen-specific T cells (major histocompatibility complex tetramer staining), the ability of neoantigen-specific T cells to secrete IFN-$\gamma$ (ELISPOT assay) and the ability of neoantigen-specific T cells to kill OVCAR-8 ovarian cancer cells *in vitro* (cytotoxicity assay). CUD-002 products derived from six donors had these pairwise data. We found that the percentage of non-dendritic cells did not correlate with the percentage of neoantigen-specific T cells (Figure 5D), IFN-$\gamma$ secretion (Figure 5E) or T-cell cytotoxicity (Figure 5F). Taken together, we concluded that non-dendritic cells present in CUD-002 product did not alter the anti-tumor ability of dendritic cells.

### *Tumorigenicity and toxicity tests of CUD-002 product in mice*

We examined tumorigenicity and toxicity of CUD-002 product. Using Click-iT EdU cell proliferation assay, we found negligible incorporation of EdU into CUD-002 product (Figure 6A). Consistently, single-cell RNA-sequencing analysis revealed that cell-cycle gene expression signature were absent in all cell types except for the HSC population (Figure 6B). The frequency of HSC was typically less than 0.1% in CUD-002 product. These results indicate that the tumorigenic potential of CUD-002 should be negligible. In accordance with NMPA guidelines to develop cell therapy, the tumorigenic potential and toxicity profiles of CUD-002 product in vivo were assessed by an independent contractor. HeLa cells or CUD-002 product were injected subcutaneously into flanks of NOD mice, respectively, and tumor size was measured every week for eight weeks. As expected, 100% of NOD mice inoculated with HeLa cells developed palpable tumors (n = 12). In contrast, no detectable tumors were formed in mice injected with CUD-002 product at any time during an 8-week period (n = 24) (Figure 6C). CUD-002 also did not form any tumors after 112 days (n = 24). In a separate experiment to examine *in vivo* toxicity profiles, no overt adverse effects were reported by the independent contractor, as mice injected with CUD-002 product exhibited normal tissue architecture as well as normal clinical parameters (n = 60) (Figure 6D).

## Discussion

Successful anti-tumor immunity largely depends on the cross-presentation of tumor-derived antigens by dendritic cells to cytotoxic T cells. This principle has been exploited to develop novel therapeutics that have achieved remarkable clinical efficacies in human cancers. The first cell-based immunotherapy approved by the US Food and Drug Administration to treat cancer is Sipuleucel-T, also known as PROVENGE or Dendreon, a dendritic cell–based cytotherapy. Since then, dendritic cells have been used as vessels to load tumor-specific antigens to treat cancer patients in many clinical trials. These trials have collectively demonstrated that dendritic cell–based therapies

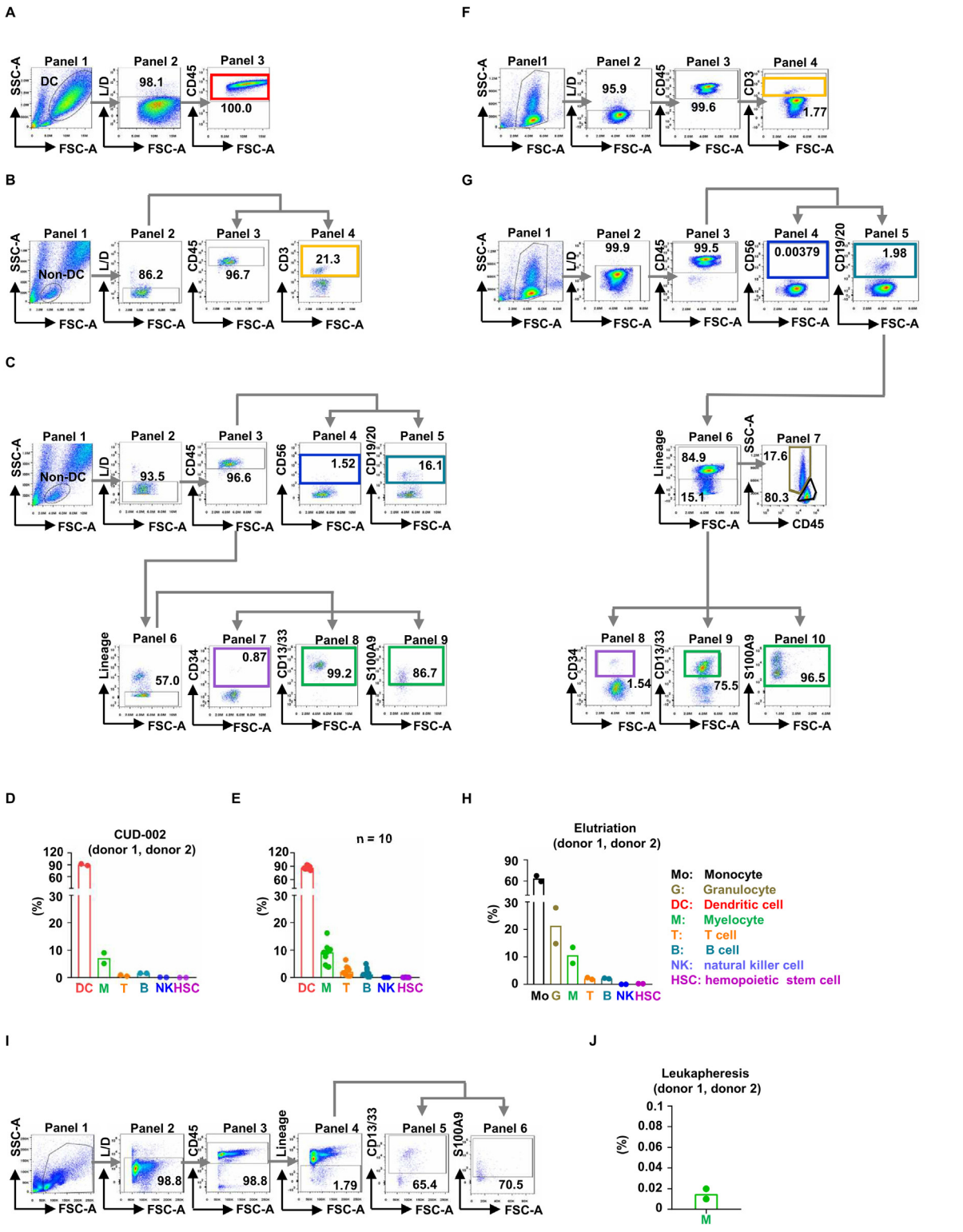


**Figure 4.** Verification by FACS of cell types identified by single-cell transcriptomic analysis. (A) Gating strategy of FACS analyses to quantitate dendritic cells (DCs) in CUD-002. Cells were gated based on side scatter area (SSC-A) and forward scatter area (FSC-A) (panel 1), then gated to identify live cells (panel 2) and CD45+ cells (panel 3). (B) Gating strategy to quantitate T cells in CUD-002. Non-DCs were gated based on SSC-A and FSC-A (panel 1), then gated to identify live cells (panel 2) and CD45+ cells (panel 3). CD45+ cells were further gated to identify CD3+ T cells (panel 4). (C) Gating strategy to quantitate NK, B, HSC and myelocyte in CUD-002. Non-DC cells were gated based on SSC-A and FSC-A (panel 1), then gated to identify live cells (panel 2) and CD45+ cells (panel 3). CD45+ cells were further gated to identify CD56+ NK cells (panel 4) and CD19+CD20+ B cells (panel 5). To quantify hemopoietic stem cell and myelocyte, live cells (panel 2) and CD45+ cells (panel 3) were gated for lineage-negative cells (CD3, CD16, CD19, CD20, CD56 and CD14) (panel 6). Lineage-negative cells were then gated to identify CD34+ hemopoietic stem cells (panel 7) and CD13+CD33+ S100A9+ myelocyte cells (panel 8 and 9). (D) The frequencies of indicated cell types in CUD-002 product. Materials from the same two donors as Figure 3 were analyzed. (E) The frequencies of indicated cell types in additional 10 batches of CUD-002 product. (F) Gating strategy to quantitate T cells in elutriation product. Cells were gated based on SSC-A and FSC-A (panel 1), then gated to identify live cells (panel 2) and CD45+ cells (panel 3). CD45+ cells were further gated to identify CD3+ T cells (panel 4). (G) Gating strategy to quantitate NK, B, monocyte, granulocyte, HSC and myelocyte in elutriation product. Cells were gated based on SSC-A and FSC-A (panel 1), then gated to identify live cells (panel 2) and CD45+ cells (panel 3). CD45+ cells were further gated to identify CD56+ NK cells (panel 4) and CD19+CD20+ B cells (panel 5). To quantify hemopoietic stem cell and myelocyte, live cells (panel 2) and CD45+ cells (panel 3) were gated for lineage-negative cells

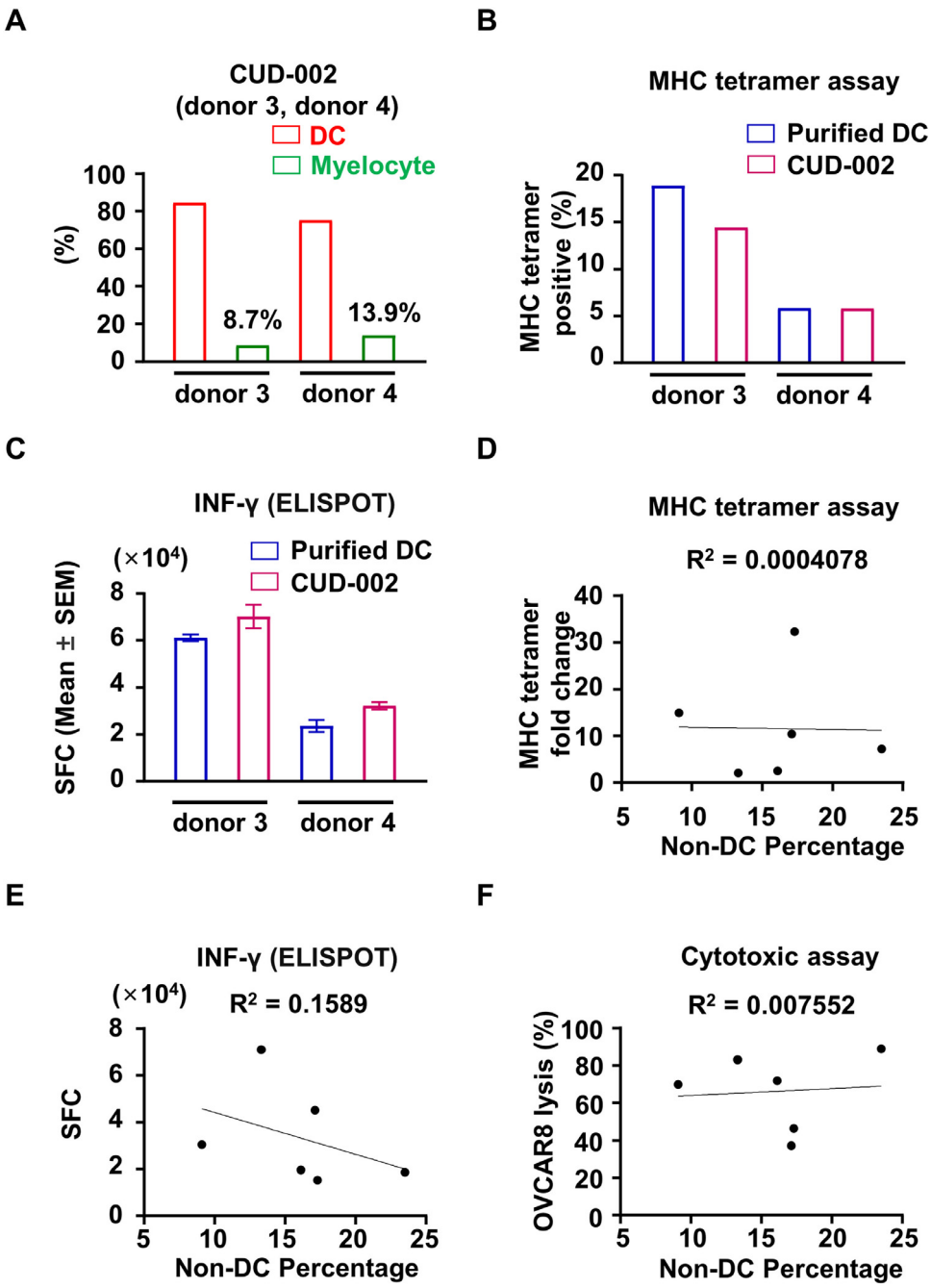


**Figure 5.** Non-dendritic cell (DC) cell types in CUD-002 do not impair the efficacy of DCs. (A) The percentage of DC and myelocyte in CUD-002 derived from donors 3 and 4. (B) The effect of non-DC cell types on the ability of CUD-002 to stimulate neoantigen-specific CD8+ T cells. DCs from CUD-002 product were affinity purified using anti-CD209 (purity > 99% by FACS analysis). CUD-002 and purified DC were compared in their abilities to stimulate antigen-specific T cell response using MART-1 as a model antigen. MART-1–specific T cells were quantified by major histocompatibility complex tetramer assay. (C) The effect of non-DC cell types on the ability of CUD-002 to stimulate IFN-$\gamma$ secretion in neoantigen-specific CD8+ T cells. MART-1–specific T cells from (B) secreted similar amount of IFN-$\gamma$ in ELISPOT assay. The number of spot-forming cells (SFCs) per 106 CD8+ T cells is shown. (D-F) Retrospective analysis of the correlation between the percentage of non-DC cells and percentage of neoantigen-specific T cells (MHC tetramer staining) (D), the ability of neoantigen-specific T cells to secrete IFN-$\gamma$ (ELISPOT assay) (E), and the ability of neoantigen-specific T cells to kill OVCAR-8 ovarian cancer cells in vitro (cytotoxicity assay) (F) (n = 6). (Color version of figure is available online.)

are usually safe in humans. However, the clinical efficacies vary among patients, suggesting that several key aspects need further optimization. In fact, there is currently no census on the best way to manufacture dendritic cells on an industrial scale.

In the present study, we demonstrate a fully developed process to reproducibly manufacture GMP-grade, therapeutic dendritic cell product (named CUD-002). CUD-002 is a versatile platform developed to load *in vitro*–transcribed mRNA encoding any tumor-specific antigens of

(CD3, CD16, CD19, CD20, CD56 and CD14) (panel 6). Lineage negative cells were then gated to identify CD34+ hemopoietic stem cells (panel 8) and CD13+CD33+ S100A9+ myelocyte cells (panel 9 and 10). Lineage-positive cells were then gated to identify CD45low granulocyte (panel 7) and CD45high monocyte (panel 7). (H) The frequencies of indicated cell types in the starting materials used for CUD-002 manufacturing. Materials from the same two donors as in Figure 3 were analyzed. (I) Gating strategy to quantitate myelocyte in leukapheresis product. Cells were gated based on SSC-A and FSC-A (panel 1), live cells (panel 2) and CD45+ cells (panel 3) were gated for lineage-negative cells (CD3, CD16, CD19, CD20, CD56 and CD14) (panel 4). Lineage negative cells were then gated to identify CD13+CD33+ S100A9+ myelocyte cells (panel 5 and 6). (J) The frequencies of myelocyte in leukapheresis product. Materials from the same two donors as in Figure 3 were analyzed. (Color version of figure is available online.)

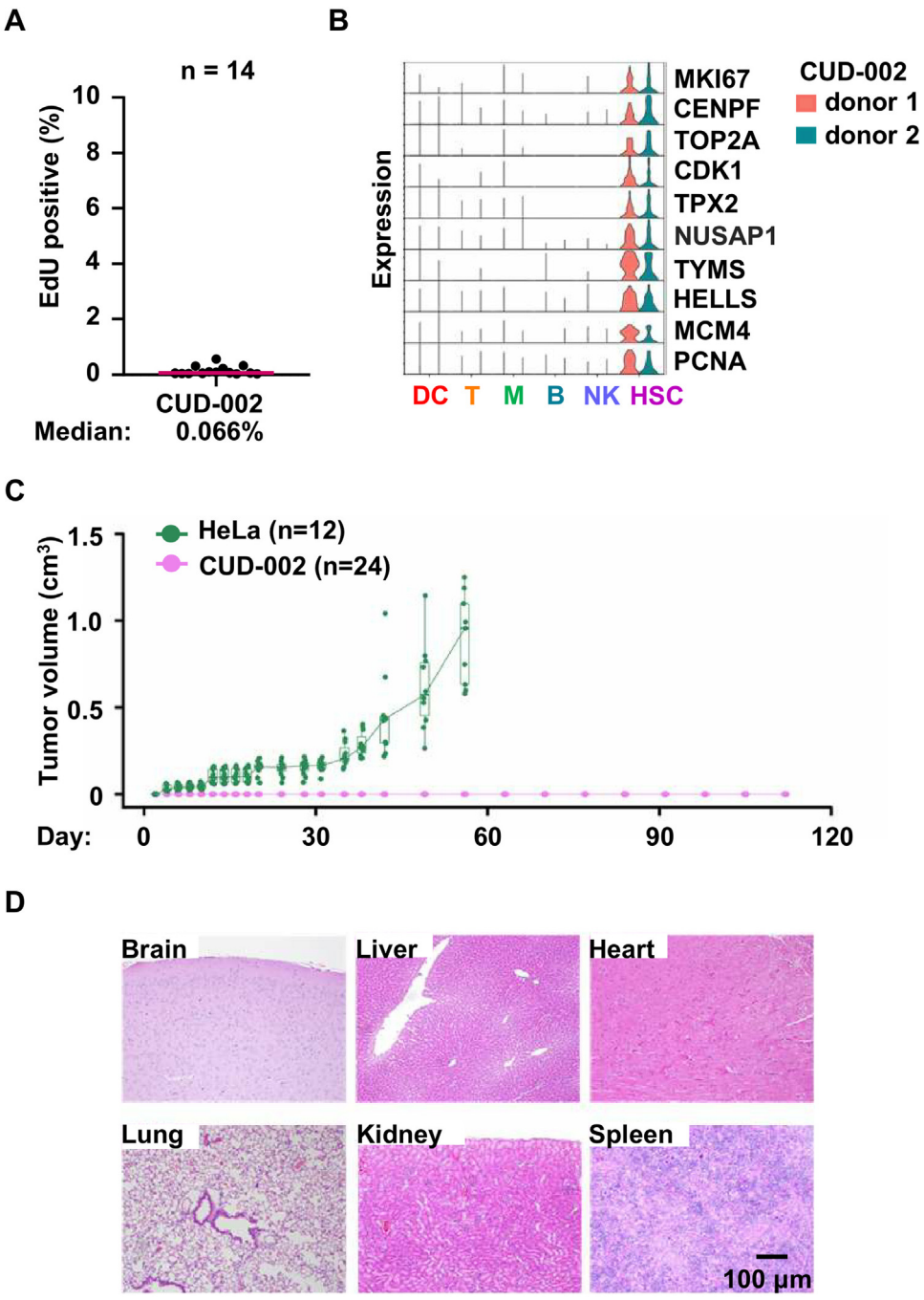


**Figure 6.** Tumorigenicity and toxicity tests of CUD-002 product. (A) EdU cell proliferation assay to analyze 14 batches of CUD-002 product, same batches as in Figure 5D. (B) Violin plot of cell-cycle gene expression signature in identified cell types in CUD-002. Note that only HSC expresses this signature. (C) Tumorigenic capacity of HeLa cells and CUD-002 product. HeLa cells were subcutaneously inoculated in non-obese diabetic mice as positive control (n = 11). CUD-002 product was inoculated the same way (n = 24). This experiment was carried out by an independent contractor. (D) Toxicity test of CUD-002 product. Mice were injected with eight doses of CUD-002 product, and evaluated after 65 days. Examples of hematoxylin and eosin staining of representative tissues were shown. (Color version of figure is available online.)

interest, and its efficacy is under clinical evaluation (NCT05270720). To manufacture CUD-002, peripheral blood monocytes are first collected by leukapheresis and then enriched by elutriation. Alternatively, antibody-based affinity purification strategy also can be used to enrich monocytes after leukapheresis. Elutriation is cheaper and requires fewer handing steps, although the resulting monocyte purity may be slightly lower than affinity purification with anti-CD14 antibodies. However, anti-CD14 antibodies may have the potential to activate monocytes [4,23]. Here, we demonstrate that we have established a robust manufacturing process to produce dendritic cells with high efficiency using materials from more than a hundred donors. Regardless of elutriation or affinity purification, the final product inevitably contains cell types other than dendritic cells. The heterogeneity in cell type composition may elicit regulatory concerns. Using single-cell transcriptomic profiling, we identify lymphocyte, myelocyte and trace amount of NK and HSC present in CUD-002. These cells likely originate from leukapheresis product because we can detect their presence by FACS analysis. Single-cell sequencing and FACS analysis also demonstrate a complete absence of monocytes and granulocytes in CUD-002. These two cell types are the most abundant ones in leukapheresis product, further demonstrating a highly efficient manufacturing process. We anticipate that single-cell sequencing will become an indispensable tool to guide the development of manufacturing process to ensure reproducibility and high quality for cytotherapies.

## Funding

This work was supported by the National Natural Science Foundation of China (31971141 and 32271348) and the Science and Technology Department of Sichuan Province (2021YJ0012).

## Declaration of Competing Interest

The authors have no commercial, proprietary or financial interest in the products or companies described in this article.

## Author Contributions

Conception and design of the study: PD, PB and QL. Acquisition of data: QL, RY, JJ, HT, PL, XZ and TL. Analysis and interpretation of data: CY, PB and QL. Drafting or revising the manuscript: QL and QL. All authors have approved the final article.

## Data and Materials Availability

All data needed to evaluate the conclusions in the paper are present in the paper. Additional data related to this paper may be requested from the corresponding authors.

## References

[1] Wculek SK, et al. Dendritic cells in cancer immunology and immunotherapy. Nat Rev Immunol 2020;20(1):7–24.
[2] Blander JM. Regulation of the Cell Biology of Antigen Cross-Presentation. Annu Rev Immunol 2018;36:717–53.
[3] Perez CR, De Palma M. Engineering dendritic cell vaccines to improve cancer immunotherapy. Nat Commun 2019;10(1):5408.
[4] Hopewell EL, Cox C. Manufacturing Dendritic Cells for Immunotherapy: Monocyte Enrichment. Mol Ther Methods Clin Dev 2020;16:155–60.
[5] Harari A, et al. Antitumour dendritic cell vaccination in a priming and boosting approach. Nat Rev Drug Discov 2020;19(9):635–52.
[6] Cheever MA, Higano CS. PROVENGE (Sipuleucel-T) in prostate cancer: the first FDA-approved therapeutic cancer vaccine. Clin Cancer Res 2011;17(11):3520–6.
[7] Sabado RL, Balan S, Bhardwaj N. Dendritic cell-based immunotherapy. Cell Res 2017;27(1):74–95.
[8] Lheureux S, et al. Epithelial ovarian cancer. Lancet 2019;393(10177):1240–53.
[9] Zhang L, et al. Intratumoral T cells, recurrence, and survival in epithelial ovarian cancer. N Engl J Med 2003;348(3):203–13.
[10] Matulonis UA, et al. Antitumor activity and safety of pembrolizumab in patients with advanced recurrent ovarian cancer: results from the phase II KEYNOTE-100 study. Ann Oncol 2019;30(7):1080–7.
[11] Moore KN, et al. Atezolizumab, Bevacizumab, and Chemotherapy for Newly Diagnosed Stage III or IV Ovarian Cancer: Placebo-Controlled Randomized Phase III Trial (IMagyn050/GOG 3015/ENGOT-OV39). J Clin Oncol 2021;39(17):1842–55.
[12] Monk BJ, et al. Chemotherapy with or without avelumab followed by avelumab maintenance versus chemotherapy alone in patients with previously untreated epithelial ovarian cancer (JAVELIN Ovarian 100): an open-label, randomised, phase 3 trial. Lancet Oncol 2021;22(9):1275–89.
[13] Fucikova J, et al. Immunological control of ovarian carcinoma by chemotherapy and targeted anticancer agents. Trends Cancer 2022;8(5):426–44.
[14] Vonderheide RH. The Immune Revolution: A Case for Priming, Not Checkpoint. Cancer Cell 2018;33(4):563–9.
[15] Zheng GX, et al. Massively parallel digital transcriptional profiling of single cells. Nat Commun 2017;8:14049.
[16] Xu K, et al. Single-cell RNA sequencing reveals cell heterogeneity and transcriptome profile of breast cancer lymph node metastasis. Oncogenesis 2021;10(10):66.
[17] McGinnis CS, Murrow LM, Gartner ZJ. DoubletFinder: Doublet Detection in Single-Cell RNA Sequencing Data Using Artificial Nearest Neighbors. Cell Syst 2019;8(4):329-337.e4.
[18] Hao Y, et al. Integrated analysis of multimodal single-cell data. Cell 2021;184(13):3573-3587.e29.
[19] Becht E, et al. Dimensionality reduction for visualizing single-cell data using UMAP. Nat Biotechnol 2018.
[20] Korsunsky I, et al. Fast, sensitive and accurate integration of single-cell data with Harmony. Nat Methods 2019;16(12):1289–96.
[21] Stuart T, et al. Comprehensive Integration of Single-Cell Data. Cell 2019;177(7):1888-1902.e21.
[22] Aran D, et al. Reference-based analysis of lung single-cell sequencing reveals a transitional profibrotic macrophage. Nat Immunol 2019;20(2):163–72.
[23] Wu Z, et al. CD14: Biology and role in the pathogenesis of disease. Cytokine Growth Factor Rev 2019;48:24–31.